Finite-element analysis of quantum wires with arbitrary cross sections

Ogawa, Matsuto

Kunimasa, T.

Ito, M.

Miyoshi, Tanroku

(Citation)
Journal of Applied Physics,84(6):3242-3249

(Issue Date)
1998-09-15

(Resource Type)
journal article

(Version)
Version of Record

(URL)
https://hdl.handle.net/20.500.14094/90000826

Finite-element analysis of quantum wires with arbitrary cross sections

M. Ogawa,[a] T. Kunimasa, T. Ito, and T. Miyoshi
Department of Electrical and Electronics Engineering, Kobe University, 1 Rokkodai, Nada, Kobe 657, Japan

(Received 20 April 1998; accepted for publication 9 June 1998)

A finite-element method is developed for the analysis of eigenstates in the valence band of quantum wires which have arbitrary potential profiles. Our method is basically based on the Galerkin procedure and triangle linear elements are used as finite elements. In our formulation the effect of the band mixing in the valence band is duly taken into account. Boundary conditions at heterointerfaces are also taken into account in the multiband envelope function space. Numerical examples are presented for circular, square, rectangular, and triangular quantum wire structures. The relation is clarified between the degeneracy in the E-k_y dispersion curve and the symmetricity of the confinement potential. © *1998 American Institute of Physics.* [S0021-8979(98)02018-0]

I. INTRODUCTION

Recent development in epitaxial crystal growth techniques such as molecular-beam epitaxy (MBE) and metalorganic chemical vapor deposition (MOCVD) has enabled us to fabricate a high quality of quantum structures such as quantum wells (QWs), quantum wires (QWRs) and quantum dots (QDs). Specifically, QWR structures have been attracting much attention, since they are promising for possible low-threshold lasers and polarization-stabilized vertical cavity surface-emitting lasers (VCSELs).

So far, various kinds of QWRs with various cross sections[1–4] were studied to fabricate uniformly high density QWRs and achieve successful application to QWR lasers. In the valence band of such QWRs, a reduction of the dimensionality enhances the heavy hole (HH) and light hole (LH) mixing and increases the nonparabolicities compared with those of quantum wells. These changes strongly depend on the confinement potential, that is, the cross-sectional shapes of the QWRs.[5] Therefore, it is quite important to precisely analyze and design the valence subband structures of QWRs with arbitrary cross sectional shapes for optimal design of QWR optical devices. Recently, Ji *et al.* developed a sophisticated method to analyze both quantum bound states and current-carrying states in two-dimensional quantum structures based on the mode matching method at boundaries and the finite-element method.[6] Lent *et al.* also developed a sophisticated procedure to analyze current-carrying states in such structures based on the quantum transmitting boundary method.[7,8] However, their procedure has concentrated only on the analysis of the behavior of the conduction electrons where the possible effect of the band mixing is neglected.

In this paper, we present a calculation procedure based on a finite-element method to analyze electronic states of QWRs. We have paid attention to the effect of the band mixing in the valence band on the valence-subband structures of a QWR with an arbitrary cross section. In our calculation, the multiband-effective-mass theory[9] is adopted where the effect of the valence-band mixing, continuity of the probability-current densities, and the effect of the finite-potential confinement of carriers between the QWR and the barriers are rigorously considered in the $\boldsymbol{k}$-dependent multiband space. Our procedure is a natural extension of the works of Ji and Lent to the multiband space, although our analysis is carried out for the bounded states in the valence band of QWRs. Numerical examples of triangular, rectangular, and circular cross-sectional shape QWRs are presented.

II. BASIC EQUATIONS

First, we consider a [0 1 0]-oriented semiconductor QWR as shown in Fig. 1. For calculation of the optical properties, it is necessary to know both the subband structures (E-k_y dispersion relations) and the wave functions of carriers in the QWR. In calculating the hole states, we assume that the conduction and valence bands are decoupled since the band gap is sufficiently large compared with the subband separation in ordinary GaAs/AlGaAs QWR systems. To calculate the electron states in the conduction band, we have only to use the effective mass approximation and ignore the mixing effect in what follows.

The valence-subband structures of a [0 1 0]-oriented semiconductor QWR can be calculated by solving the multiband-effective-mass equation[9,10] for

$$|1{:}\mathrm{HH}\rangle\ |2{:}\mathrm{LH}\rangle\ |3{:}\mathrm{LH}\rangle\ |4{:}\mathrm{HH}\rangle$$

$$\begin{pmatrix} H_{\mathrm{HH}} & c & b & 0 \\ c^{\dagger} & H_{\mathrm{LH}} & 0 & -b \\ b^{\dagger} & 0 & H_{\mathrm{LH}} & c \\ 0 & -b^{\dagger} & c^{\dagger} & H_{\mathrm{HH}} \end{pmatrix} \boldsymbol{G} = E(k_y)\boldsymbol{G}, \tag{1}$$

$$\boldsymbol{G} = (G_1, G_2, G_3, G_4)^T, \tag{2}$$

where the basis vectors $|j\rangle$ ($j=1,2,3,4 \in \{u_{3/2,\mathbf{0}}, u_{3/2,\mathbf{0}}, u_{-1/2,\mathbf{0}}, u_{-3/2,\mathbf{0}}\}$) are the cell-periodic part of the four degenerate Bloch wave functions at the Brillouin zone center and the spin-orbit split-off band is ignored and $\boldsymbol{G}$ is an en-

[a]Author to whom correspondence should be addressed; electronic mail: ogawa@eedept.kobe-u.ac.jp

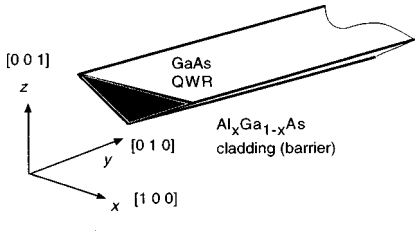

FIG. 1. A [010] oriented GaAs quantum wire structure with a triangular cross section. The energy barrier of the cladding region is assumed to be made of $Al_{0.4}Ga_{0.6}As$.

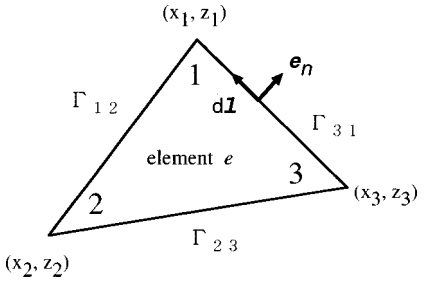

FIG. 2. A linear triangular element for the finite element method. Γ_{ij} $(i,j=1,2,3)$ denote boundaries between the neighboring elements. $d\boldsymbol{l}$ is a unit tangential vector along Γ_{31} and $\boldsymbol{e}_n$ is the unit normal vector.

velope function vector. The wave function Ψ_v of holes in the valence band is expressed with the envelope functions G_j and the basis functions $|j\rangle$ as

$$\boldsymbol{\Psi}_v(x,y,z;k_y)=\sum_{j=1}^{4} G_j(x,z;k_y)\exp(k_y y)|j\rangle. \tag{3}$$

All matrix elements in the Hamiltonian are written in terms of Luttinger parameters γ_1, γ_2, and γ_3:[9]

$$H_{\mathrm{HH}}=-\frac{\hbar^2}{2m_0}[(\gamma_1+\gamma_2)(k_x^2+k_y^2)+(\gamma_1-2\gamma_2)k_z^2]+V(x,z),$$

$$H_{\mathrm{LH}}=-\frac{\hbar^2}{2m_0}[(\gamma_1-\gamma_2)(k_x^2+k_y^2)+(\gamma_1+2\gamma_2)k_z^2]+V(x,z), \tag{4}$$

$$b=\frac{\hbar^2}{m_0}\sqrt{3}\gamma_3(k_x-ik_y)k_z,$$

$$c=\frac{\hbar^2}{2m_0}\sqrt{3}[\gamma_2(k_x^2-k_y^2)-2i\gamma_3 k_x k_y],$$

where m_0 is the free electron mass, $\hbar$ is Plank's constant divided by 2π, $k_i(i=x,y,z)$ is the wave number, and $V(x,z)$ is the confinement potential. In the QWR, the wave numbers k_x and k_z are substituted by operators as $k_x\rightarrow -i\partial/\partial x$ and $k_z\rightarrow -i\partial/\partial z$, respectively, since the system is quantized in the x and z directions. We have to be careful that these substitutions are done to preserve the Hermiticity of the Hamiltonian, that is, these elements should have the forms:

$$H_{\mathrm{HH}}=\frac{\hbar^2}{2m_0}\left[\left(\frac{\partial}{\partial x}(\gamma_1+\gamma_2)\frac{\partial}{\partial x}-(\gamma_1+\gamma_2)k_y^2\right)+\frac{\partial}{\partial z}(\gamma_1-2\gamma_2)\frac{\partial}{\partial z}\right]+V(x,z),$$

$$H_{\mathrm{LH}}=\frac{\hbar^2}{2m_0}\left[\left(\frac{\partial}{\partial x}(\gamma_1-\gamma_2)\frac{\partial}{\partial x}-(\gamma_1-\gamma_2)k_y^2\right)+\frac{\partial}{\partial z}(\gamma_1+2\gamma_2)\frac{\partial}{\partial z}\right]+V(x,z), \tag{5}$$

$$b=-\frac{\hbar^2}{2m_0}\sqrt{3}\left(\frac{\partial}{\partial x}+k_y\right)\left(\gamma_3\frac{\partial}{\partial z}+\frac{\partial}{\partial z}\gamma_3\right),$$

$$c=-\frac{\hbar^2}{2m_0}\sqrt{3}\left[\left(\frac{\partial}{\partial x}\gamma_2\frac{\partial}{\partial x}-\gamma_2 k_y^2\right)+k_y\left(\gamma_3\frac{\partial}{\partial x}+\frac{\partial}{\partial x}\gamma_3\right)\right].$$

The Hermiticity of the Hamiltonian of the system ensures conservation of probability-current densities at the heterointerface as will be discussed in Sec. III.

III. METHOD OF ANALYSIS

A. Finite-element method (FEM)

In this paper, we confine ourselves in an analysis of electronic states in a QWR, specifically in the valence band where the band-mixing effect is significant. Since the envelope functions $G_j(x,z)$ should satisfy $G_j\rightarrow 0(x,z\rightarrow\pm\infty)$, we can approximate that the envelope functions vanish at a certain extent of x and z and the boundary conditions are given by

$$G_j(x_l,z)=G_j(x_u,z)=0,$$
$$G_j(x,z_l)=G_j(x,z_u)=0, \quad (j=1,\cdots,4), \tag{6}$$

where the region defined by $x_l\leqslant x\leqslant x_u$ and $z_l\leqslant z\leqslant z_u$ is a sufficiently wide domain which includes the QWR structure under consideration.

Dividing the region into a number of linear triangle elements in Fig. 2, where x_i and z_i $(i=1, 2,3)$ denote the coordinates at each elemental node, the envelope function within each element is defined in terms of the values of envelope functions at the nodal points $\{G_j\}_e$. Since we can reduce the degree of the differential in the Hamiltonian by integrating by part in Eq. (9), we can use the *linear* element.

The magnitude of the envelope function of holes G_{je} in an element e is approximated by

$$G_{je}=\{N\}^T\{G_j\}_e=\{G_j\}_e^T\{N\}, \tag{7}$$

where $\{N\}$ is a shape function as will be defined in Eq. (11).

Then the multiband effective mass equation (1) becomes

$$\sum_{j'} \int\int_e \{N\}H_{jj'}\{N\}^T\{G_j\}_e dx\, dz = E\int\int_e \{N\}\{N\}^T\{G_j\}_e dx\, dz. \tag{8}$$

We define the matrices $\{H_{jj'}\}$ and $\{M\}$

$$\{H_{jj'}\}_e = \int\int_e \{N\}H_{jj'}\{N\}^T dx\, dz, \qquad \{M\}_e = \int\int_e \{N\}\{N\}^T dx\, dz. \tag{9}$$

Then the element equation is expressed as

$$\sum_{j'} \{H_{jj'}\}_e\{G_{j'}\}_e = E\{M\}_e\{G_j\}_e. \tag{10}$$

In the discretization, the shape function $\{N\}$ is given by

$$\{N\} = \frac{1}{A_e}\begin{bmatrix} a_1 & b_1 & c_1 \\ a_2 & b_2 & c_2 \\ a_3 & b_3 & c_3 \end{bmatrix}\begin{bmatrix} 1 \\ x \\ z \end{bmatrix}, \tag{11}$$

where

$$\begin{aligned} &a_1 = x_2z_3 - x_3z_2, \quad b_1 = z_2 - z_3, \quad c_1 = x_3 - x_2, \\ &a_2 = x_3z_1 - x_1z_3, \quad b_1 = z_3 - z_1, \quad c_2 = x_1 - x_3, \\ &a_3 = x_1z_2 - x_2z_1, \quad b_1 = z_1 - z_2, \quad c_1 = x_2 - x_1, \end{aligned} \tag{12}$$

and A_e is area of each element e

$$A_e = \frac{1}{2}\begin{vmatrix} 1 & 1 & 1 \\ x_1 & x_2 & x_3 \\ z_1 & z_2 & z_3 \end{vmatrix}. \tag{13}$$

The matrix elements in Eq. (10) are expressed as

$$\{H_{\mathrm{HH}}\}_{ij} = -\frac{\hbar^2}{2m_0}\left[\frac{b_ib_j}{4A_e}(\gamma_1+\gamma_2) + \frac{(1+\delta_{ij})A_e}{12}(\gamma_1+\gamma_2)k_y^2 + \frac{c_ic_j}{4A_e}(\gamma_1 - 2\gamma_2)\right] + \frac{(1+\delta_{ij})A_e}{12}V(x,z),$$

$$\{H_{\mathrm{LH}}\}_{ij} = -\frac{\hbar^2}{2m_0}\left[\frac{b_ib_j}{4A_e}(\gamma_1-\gamma_2) + \frac{(1+\delta_{ij})A_e}{12}(\gamma_1-\gamma_2)k_y^2 + \frac{c_ic_j}{4A_e}(\gamma_1 + 2\gamma_2)\right] + \frac{(1+\delta_{ij})A_e}{12}V(x,z), \tag{14}$$

$$\{b\}_{ij} = \frac{\sqrt{3}\hbar^2}{m_0}\gamma_3\left(\frac{b_ic_j + c_ib_j}{8A_e} + \frac{c_i - c_j}{12}k_y\right),$$

$$\{c\}_{ij} = \frac{\sqrt{3}\hbar^2}{2m_0}\left[\frac{b_ib_j}{4A_e}\gamma_2 - \frac{(1+\delta_{ij})A_e}{12}k_y^2\gamma_2 + \frac{b_i - b_j}{6}\gamma_3k_y\right],$$

where $\{b^\dagger\}_{ij} = \{b\}^*_{ji}$ and $\{c^\dagger\}_{ij} = \{c\}^*_{ji}$.

Finally the element equations are summed up into a total generalized eigenvalue equation:

$$[H][G] = E[M][G]. \tag{15}$$

In this equation total matrices $[H]$, $[M]$, and $[G]$ are $n \times n$ matrices with n nodes in the system under consideration. They are defined as

$$[H] = \begin{bmatrix} \{H_{11}^{4\times4}\} & \{H_{12}^{4\times4}\} & \{H_{13}^{4\times4}\} & \cdots & \{H_{1n}^{4\times4}\} \\ \{H_{21}^{4\times4}\} & \{H_{22}^{4\times4}\} & \{H_{23}^{4\times4}\} & \cdots & \{H_{2n}^{4\times4}\} \\ & \vdots & & \cdots & \vdots \\ \{H_{n1}^{4\times4}\} & \{H_{n2}^{4\times4}\} & \{H_{n3}^{4\times4}\} & \cdots & \{H_{nn}^{4\times4}\} \end{bmatrix}$$

$$[M] = \begin{bmatrix} \{M_{11}^{4\times4}\} & \{M_{12}^{4\times4}\} & \{M_{13}^{4\times4}\} & \cdots & \{M_{1n}^{4\times4}\} \\ \{M_{21}^{4\times4}\} & \{M_{22}^{4\times4}\} & \{M_{23}^{4\times4}\} & \cdots & \{M_{2n}^{4\times4}\} \\ & \vdots & & \cdots & \vdots \\ \{M_{n1}^{4\times4}\} & \{M_{n2}^{4\times4}\} & \{M_{n3}^{4\times4}\} & \cdots & \{M_{nn}^{4\times4}\} \end{bmatrix}$$

$$[G] = [G^1_{3/2}G^1_{-1/2}G^1_{1/2}G^1_{-3/2}G^2_{3/2}G^2_{-1/2}G^2_{1/2}G^2_{-3/2} \cdots G^n_{3/2}G^n_{-1/2}G^n_{1/2}G^n_{-3/2}]^T, \tag{16}$$

where the script n denotes the node number and $H^{4\times4}$ implies the 4×4 Luttinger–Kohn Hamiltonian.

B. Boundary conditions at a heterointerface

Probability current density $\boldsymbol{j}$ should be conserved at a heterointerface which imposes the boundary conditions at the interface. Probability current density is defined by

$$\boldsymbol{j} = \frac{1}{m_0}\mathbf{Re}\left(\Psi_v^*(\boldsymbol{r})\frac{\hbar}{i}\Psi_v(\boldsymbol{r})\right), \tag{17}$$

which can be straightforwardly expressed in the multiband effective mass space as

$$j_\alpha = \mathbf{Re}\left[\sum_{\beta=x,y,z}\sum_{j,j'=1}^{4}\left(\frac{1}{\hbar^2}G_j^*(D_{jj'}^{\alpha\beta} + D_{jj'}^{\beta\alpha})p^\beta G_{j'}\right)\right] \quad (\alpha = x,y,z). \tag{18}$$

Here $D_{jj'}^{\alpha\beta}$ is an effective mass tensor defined by

$$D_{jj'}^{\alpha\beta} = \frac{\hbar^2}{2m}\left(\delta_{jj'}\delta_{\alpha\beta} + \sum_{n\neq\nu}\frac{2P_{jn}^\alpha P_{nj'}^\beta}{m(\epsilon_\nu - \epsilon_n)}\right), \qquad P_{jn}^\alpha \equiv \langle u_{j0}|p_\alpha|u_{n0}\rangle_{\mathrm{UC}}, \tag{19}$$

where the momentum matrix element P_{jn}^α is calculated in a unit cell (UC).

The current density can be expressed by a matrix form

$$j_\alpha = \mathbf{Re}(\boldsymbol{G}^+\boldsymbol{J}_\alpha\boldsymbol{G}), \qquad (\boldsymbol{J}_\alpha)_{jj'} = \frac{1}{\hbar}\sum_{\beta=x,y,z}(D_{jj'}^{\alpha\beta} + D_{jj'}^{\beta\alpha})k_\beta. \tag{20}$$

Here the current-density operator matrix $\boldsymbol{J}_\alpha$ in each direction $(\alpha = x,y,z)$ is given by

$$J_x=\frac{\hbar}{m_0}\begin{pmatrix}(\gamma_1+\gamma_2)k_x & -\sqrt{3}\gamma_3 k_z & \sqrt{3}(-\gamma_2 k_x+i\gamma_3 k_y) & 0\\ -\sqrt{3}\gamma_3 k_z & (\gamma_1-\gamma_2)k_x & 0 & \sqrt{3}(-\gamma_2 k_x+i\gamma_3 k_y)\\ \sqrt{3}(-\gamma_2 k_x-i\gamma_3 k_y) & 0 & (\gamma_1-\gamma_2)k_x & \sqrt{3}\gamma_3 k_z\\ 0 & \sqrt{3}(-\gamma_2 k_x-i\gamma_3 k_y) & \sqrt{3}\gamma_3 k_z & (\gamma_1+\gamma_2)k_x\end{pmatrix}, \tag{21}$$

$$J_y=\frac{\hbar}{m_0}\begin{pmatrix}(\gamma_1+\gamma_2)k_y & i\sqrt{3}\gamma_3 k_z & \sqrt{3}(i\gamma_3 k_x+\gamma_2 k_y) & 0\\ -i\sqrt{3}\gamma_3 k_z & (\gamma_1-\gamma_2)k_y & 0 & \sqrt{3}(i\gamma_3 k_x+\gamma_2 k_y)\\ \sqrt{3}(-i\gamma_3 k_x+\gamma_2 k_y) & 0 & (\gamma_1-\gamma_2)k_y & -i\sqrt{3}\gamma_3 k_z\\ 0 & \sqrt{3}(-i\gamma_3 k_x+\gamma_2 k_y) & i\sqrt{3}\gamma_3 k_z & (\gamma_1+\gamma_2)k_y\end{pmatrix}, \tag{22}$$

$$J_z=\frac{\hbar}{m_0}\begin{pmatrix}(\gamma_1-2\gamma_2)k_z & -\sqrt{3}\gamma_3(k_x-ik_y) & 0 & 0\\ -\sqrt{3}\gamma_3(k_x+ik_y) & (\gamma_1+2\gamma_2)k_z & 0 & 0\\ 0 & 0 & (\gamma_1+2\gamma_2)k_z & \sqrt{3}\gamma_3(k_x-ik_y)\\ 0 & 0 & \sqrt{3}\gamma_3(k_x+ik_y) & (\gamma_1-2\gamma_2)k_z\end{pmatrix}, \tag{23}$$

respectively, where we have used the following relationship between the effective-mass tensor $D_{jj'}^{\alpha\beta}$ and the Luttinger parameters γ_i,

$$\gamma_1=\tfrac{1}{3}(D_{XX}^{xx}+2D_{XX}^{yy}),$$

$$\gamma_2=\tfrac{1}{6}(D_{XX}^{xx}-D_{XX}^{yy}), \tag{24}$$

$$\gamma_3=\tfrac{1}{6}(D_{XY}^{xy}+D_{XY}^{yx}).$$

Here X, Y, and Z denote the p-orbital Bloch functions. The wave numbers k_x and k_z are again changed into operators as $k_x\rightarrow -i\partial_x$ and $k_z\rightarrow -i\partial_z$, respectively.

Using the current density operators, the boundary conditions at the heterointerface in the multiband space are

$$\begin{cases}\boldsymbol{G}=(G_1,G_2,G_3,G_4)^T & \text{is continuous at the interface,}\\ (\boldsymbol{n}\cdot\boldsymbol{J})\boldsymbol{G} & \text{is also continuous at the interface,}\end{cases} \tag{25}$$

where $\boldsymbol{n}$ is the unit normal vector to the interface.[11]

We can show that our FEM formulation duly and automatically include the boundary conditions. Since we use the linear elements, $\boldsymbol{G}$ matches smoothly at each interface.

Let the boundary Γ_{31} be the heterointerface whose tangential vector is $d\boldsymbol{l}$ and unit normal vector is $\boldsymbol{e}_n$ as shown in Fig. 2 and the unit vectors in the x and z directions be $\boldsymbol{e}_x$ and $\boldsymbol{e}_z$, respectively. The line integrals along the boundaries Γ_{12} and Γ_{23} cancel out, because the tangential vectors have opposite direction (or sign) in the neighboring elements. Therefore, we need only consider the line integral along Γ_{31}. If we write the line integral of $\{H_{\mathrm{HH}}\}$ as $\{H_{\mathrm{HH}}\}_l$, it is given by

$$\begin{aligned}\{H_{\mathrm{HH}}\}_l=&\frac{\hbar^2}{2m_0}\left(\int_{\Gamma_{31}}(\gamma_1+\gamma_2)\{N\}\frac{\partial\{N\}^T}{\partial x}dz\right.\\ &\left.+\int_{\Gamma_{31}}(\gamma_1-2\gamma_2)\{N\}\frac{\partial\{N\}^T}{\partial z}dx\right)\{G_j\}_e\\ =&\frac{\hbar^2}{2m_0}\int_{\Gamma_{31}}\{N\}\left[\boldsymbol{e}_n\cdot\boldsymbol{e}_x(\gamma_1+\gamma_2)\frac{\partial\{N\}^T}{\partial x}\right.\\ &\left.+\boldsymbol{e}_n\cdot\boldsymbol{e}_z(\gamma_1-2\gamma_2)\frac{\partial\{N\}^T}{\partial z}\right]\{G_j\}_e d\boldsymbol{l}.\end{aligned} \tag{26}$$

On the other hand the current density is given by

$$\boldsymbol{j}=\frac{\hbar}{m_0}[-i(\gamma_1+\gamma_2)\partial_x\boldsymbol{e}_x-i(\gamma_1-2\gamma_2)\partial_z\boldsymbol{e}_z]. \tag{27}$$

From Eqs. (21) and (23), the normal component of the current density is

$$\begin{aligned}(\boldsymbol{e}_n\cdot\boldsymbol{j})G_j=&-i\frac{\hbar}{m_0}\boldsymbol{e}_n\cdot\left[\boldsymbol{e}_x(\gamma_1+\gamma_2)\frac{\partial\{N\}^T}{\partial x}\right.\\ &\left.+\boldsymbol{e}_z(\gamma_1-2\gamma_2)\frac{\partial\{N\}^T}{\partial z}\right]\{G_j\}_e.\end{aligned} \tag{28}$$

Since the term in brackets in the above equation is the same as that which appears in the integrand of Eq. (26), conservation of the current density ensures that the line integrals along Γ_{31} cancel out in our FEM formulation and *vice versa*.

IV. NUMERICAL RESULT

In order to demonstrate the versatility of the present method, we calculate the valence-subband structures of QWRs with several cross-sectional shapes: (a) circular quantum wire (CQWR), (b) square QWR (SQWR) [or (c) rectangular QWR (RQWR) which has $L_x=2L_z$], and (d) triangular QWR (TQWR) with the same cross-sectional area, as shown in Fig. 3. The material parameters used in the calculation are

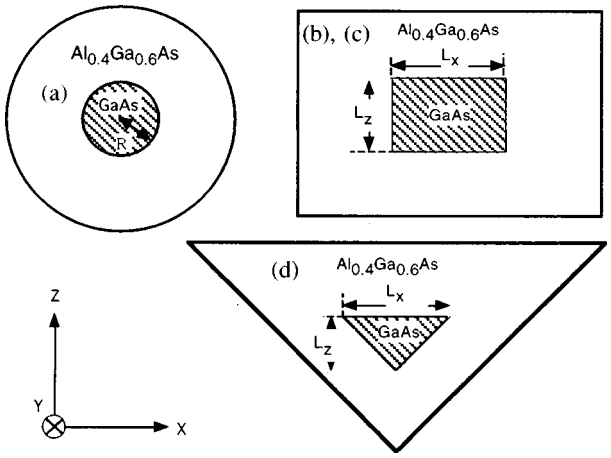

FIG. 3. Cross-sectional shapes for numerical examples: (a) circular quantum wire [CQWR: $R=6.2$ (nm)], (b) square quantum wire [SQWR: $L_x=11$(nm), $L_z=11$ (nm)], (c) rectangular quantum wire [RQWR: $L_x=15.5$ (nm), $L_z=7.7$ (nm)], (d) triangular quantum wire [TQWR: $L_x=20$ (nm), $L_z=12$ (nm)]. We have assumed those have same cross-sectional area [$S=120$ (nm^2)].

given in Table I. To solve the generalized eigenvalue problem (15), we use the Lanczos tridiagonalization method.[12]

Figures 4(a), 4(b), 4(c) and 4(d) show the E-k_y dispersion relations of several valence subbands near the valence-band top in each QWR. The calculated results for SQWR and RQWR are found to be in good agreement with those reported in the literature,[10] when the sizes are adjusted to their values.

Comparison between the dispersion relations of the CQWR and SQWR shows that they resemble each other and their 3,3′ subbands have a negative effective mass near the zone center, since the confinement potential $V(x,z)$ has similar symmetricity although the CQWR has a higher symmetricity.

Comparing the case of the SQWR and the RQWR, the dispersion curves of the SQWR cross, whereas those of the RQWR show anticrossing (see Ref. 13). This is because when the cross section is not square, the off-diagonal element of the Hamiltonian produces a repulsive interaction between the neighboring subbands.

In the CQWR, SQWR, and RQWR, since the confinement potential has symmetricity in both x and z directions,

TABLE I. Parameters used in the calculation of QWRs.

Parameter	GaAs		$Al_{0.4}Ga_{0.6}As$
E_g	1.424 eV		1.923eV
ΔE_c		0.30eV	
ΔE_v		0.20eV	
γ_1	6.85		5.16
γ_2	2.10		1.31
γ_3	2.90		2.10
m_c^*/m_0	0.067		0.117
N_p[a]		88	

[a]N_p denotes the total element number used in the calculation.

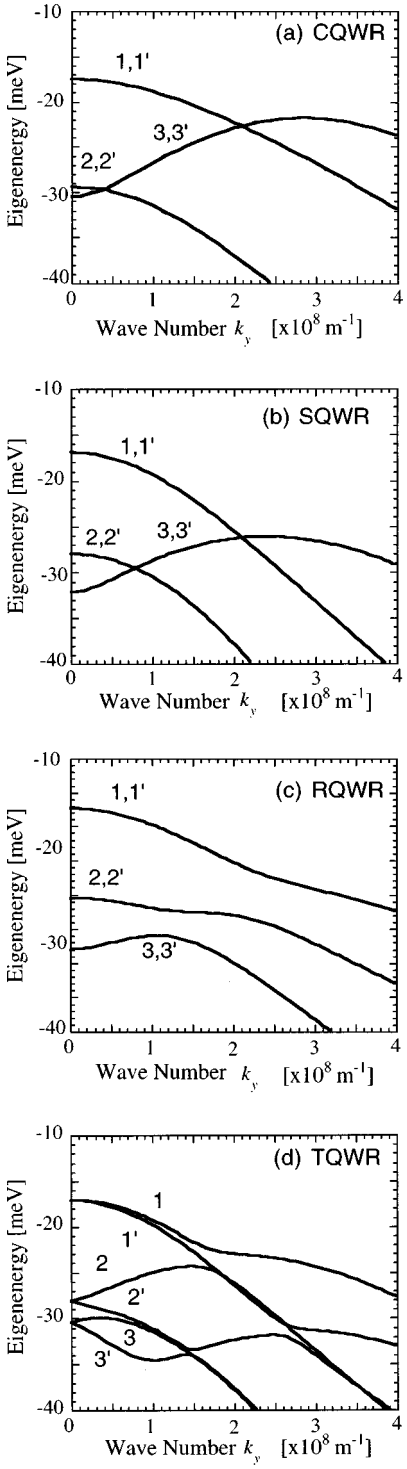

FIG. 4. (a) E-k_y dispersion relations for the CQWR, (b) those for the SQWR, (c) those for the RQWR, and (d) those for the TQWR. The origin of the hole energy is set at the valence-band top of GaAs.

that is, $V(-x,z)=V(x,z)$ and $V(x,-z)=V(x,z)$, the dispersion curves are doubly degenerated. On the other hand, in the TQWR, the dispersion curves show nondegeneracy except at the zone center ($k_y=0$). The symmetricity reflects on that of the eigenvectors as shown in Fig. 5, where (a), (b) and (c), (d) show the HH component (G_1^1 and G_4^1) and the LH component (G_2^1 and G_3^1) and its contour lines of the wave function in the lowest subband at $k_y=0$ in the SQWR, re-

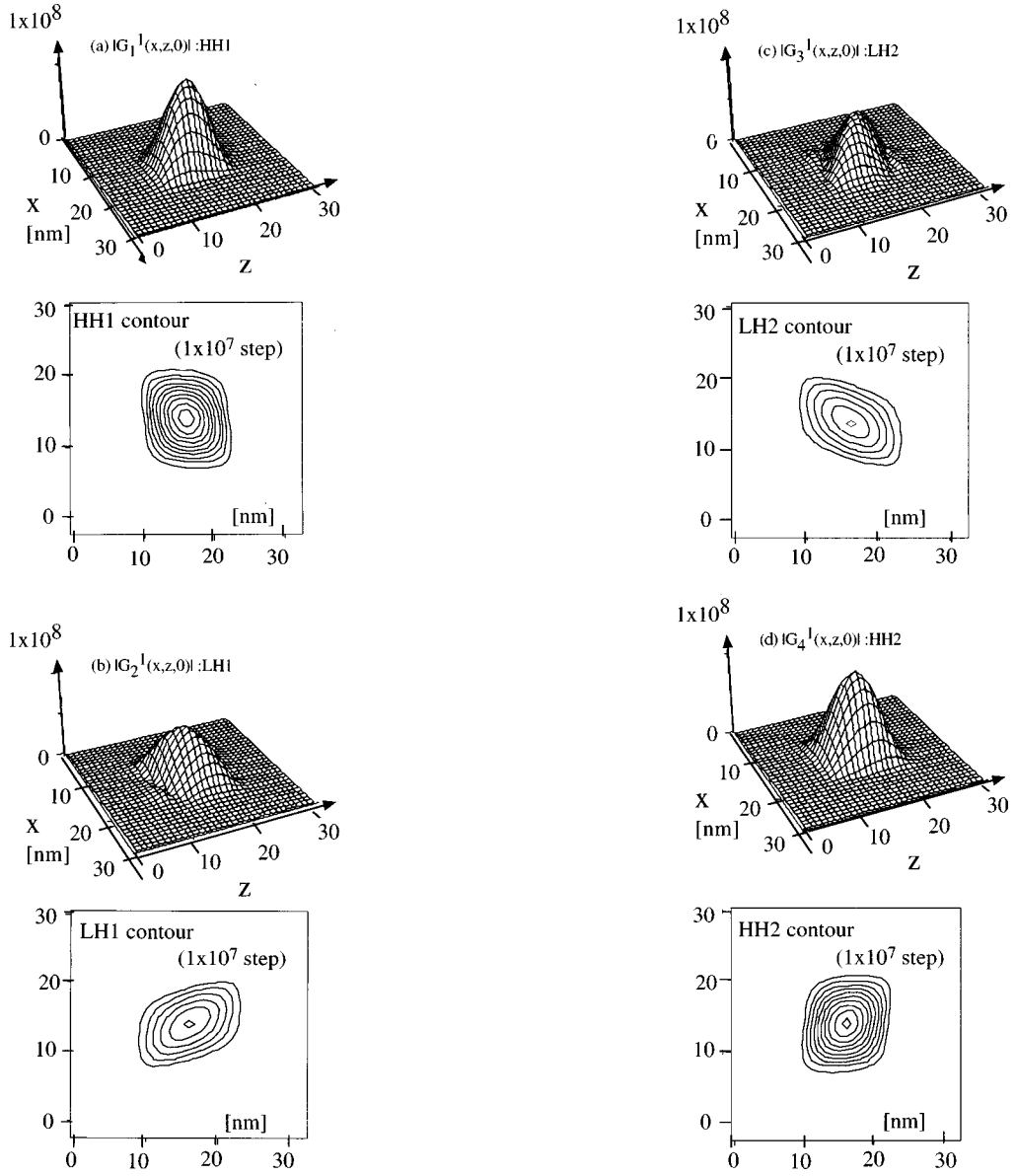

FIG. 5. (a) The heavy hole (HH) component (G_1^1) of the envelope wave function and its contour lines of the ground subband at $k_y=0$ in the SQWR. (b) The light hole (LH) (G_2^1) component and its contour lines. (c) LH (G_3^1) component and its contour lines. (d)HH (G_4^1) component and its contour lines.

spectively. As seen in the figures, G_1^1 is symmetric with G_4^1 and G_2^1 with G_3^1, respectively. Since the reduction of the dimensionality enhances the effect of the band mixing, the amplitudes of the HH and LH wave functions have nonzero values even at the zone center ($k_y=0$). In addition, the E-k_y dispersion relation of the SQWR always shows degeneracy as shown in Fig. 4(b). In the TQWR, as shown in Figs. 6(a)–6(d), the pair of G_1^1 and G_4^1 and that of G_2^1 and G_3^1 are symmetric to each other with respect to the z axis, since the confinement potential has the same symmetricity. It should be noted that we can clearly observe different symmetric properties in the envelope function depending on the symmetricity of the confinement potential in the SQWR and TQWR, although they have the same cross-sectional area. These facts can be understood as follows.

If we substitute x by $-x$ and z by $-z$ in the Hamiltonian of Eq. (1) and assume the symmetricity $V(-x,-z)=V(x,z)$ as in the case of the CQWR, SQWR, and RQWR, then the multiband-effective mass equation [Eq. (1)] becomes

$$
\begin{array}{cccc} |1\rangle & |2\rangle & |3\rangle & |4\rangle \end{array}
$$

$$
\begin{pmatrix} H_{\mathrm{HH}} & c & b & 0 \\ c^{\dagger} & H_{\mathrm{LH}} & 0 & -b \\ b^{\dagger} & 0 & H_{\mathrm{LH}} & c \\ 0 & -b^{\dagger} & c^{\dagger} & H_{\mathrm{HH}} \end{pmatrix}
\begin{pmatrix} G_4(-x,-z) \\ G_3(-x,-z) \\ -G_2(-x,-z) \\ -G_1(-x,-z) \end{pmatrix}
$$

$$
= E(k_y) \begin{pmatrix} G_4(-x,-z) \\ G_3(-x,-z) \\ -G_2(-x,-z) \\ -G_1(-x,-z) \end{pmatrix}. \tag{29}
$$

Since the envelope function vector $\boldsymbol{G}=(G_1,G_2,G_3,G_4)^T$ is

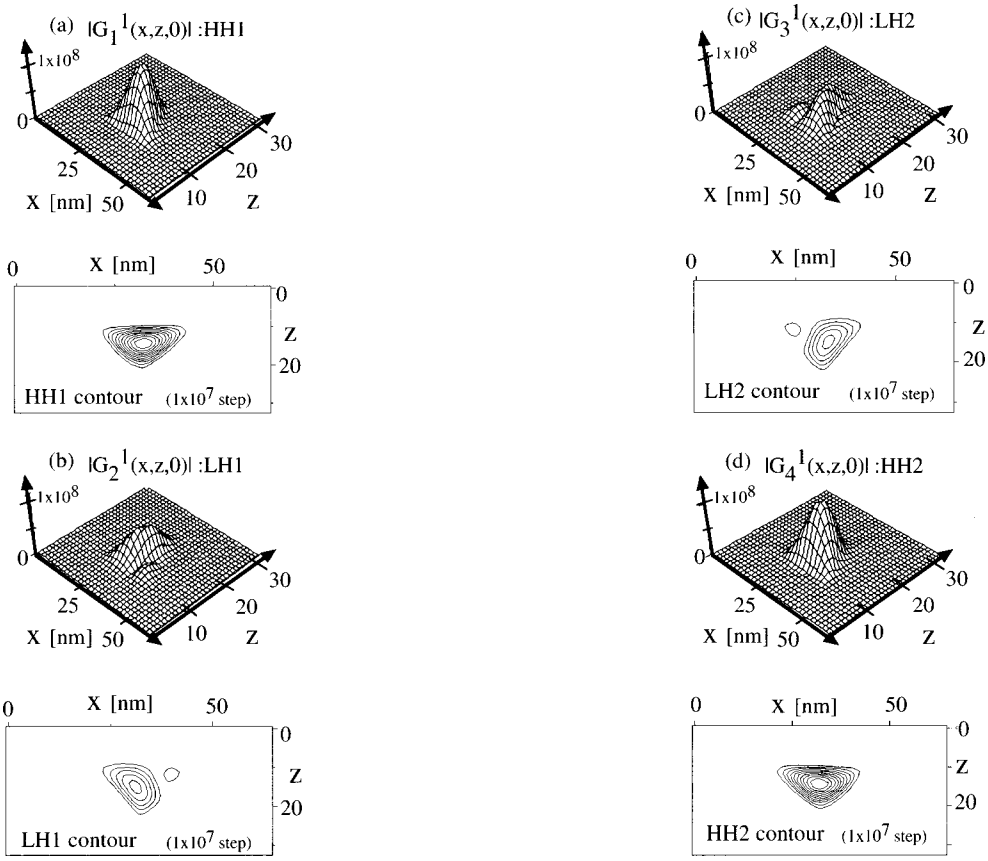

FIG. 6. (a) HH component (G_1^1) of the envelope wave function and its contour lines of the ground state at $k_y=0$ in the TQWR. (b) LH (G_2^1) component and its contour lines. (c) LH (G_3^1) component and its contour lines. (d) HH (G_4^1) component and its contour lines.

orthogonal to $\boldsymbol{G}'=[G_4(-x,-z),G_3(-x,-z),-G_2(-x,-z),-G_1(-x,-z)]^T$ and has the same eigenenergy $E(k_y)$, the dispersion curves for the CQWR, SQWR, and RQWR always show double degeneracy everywhere in the k_y space. On the contrary, the symmetricity in the confinement potential does not exist in the case of the TQWR, which results in nondegeneracy everywhere in the dispersion curve except at the zone center.

The singular dispersion relations in the TQWR may exhibit different optical properties from those of the CQWR, SQWR and RQWR, since the optical properties such as absorption spectra and gain spectra of QWRs strongly depend on the valence subband structures. In addition, optimal design of the cross-sectional shape can lead to an optimal design of QWR based optical devices since the valence-subband structures are significantly affected by the confinement potential as we have seen in the figures.

V. CONCLUSION

We have developed a finite-element method for the analysis of the valence-subband structures of GaAs/AlGaAs quantum wires with arbitrary cross-sectional shapes based on the multiband-effective mass theory. The mixing effect between the HH and LH states and the correct boundary conditions are duly included in the calculation. The validity and versatility of the method is confirmed by calculating the E-k_y dispersion relations of QWRs with various cross-sectional shapes. The relation should be emphasized between the degeneracy in the dispersion curve and the symmetricity of the confinement potential. Although we have used linear triangle elements, using higher order elements, such as the third-order Hermitian line elements, can lead to more precise calculation of eigenenergies.

Since the cross-sectional shapes are found to affect significantly the subband structures, a further study of the relationship between the cross-sectional shapes and the subband structures can lead to the optimal design of the quantum wire based optical devices.

ACKNOWLEDGMENTS

One of the authors (MO) would like to acknowledge Dr. J. A. Cullum of IBM T.J.Watson Research Center for her discussion about the Lanczos tridiagonalization procedure. This work was partially supported by a Grant-in-Aid for Scientific Research on Priority Area: ''Spin Controlled Semiconductor Nanostructures'' (Grant No. 09244215) from the Ministry of Education, Science, Sports, and Culture.

[1] L. Pfeiffer, Appl. Phys. Lett. **56**, 1697 (1990).
[2] Y. Nagamune, Y. Arakawa, S. Tsukamoto, M. Nishioka, S. Sasaki, and N. Miura, Phys. Rev. Lett. **69**, 2963 (1992).
[3] M. Higashiwaki, M. Yamamoto, T. Higuchi, S. Shimomura, A. Adachi, Y. Okamoto, N. Sano, and S. Hiyamizu, Jpn. J. Appl. Phys., Part 1 **35**, 606 (1996).
[4] K. Inoue, K. Kimura, K. Maehashi, S. Hasegawa, H. Nakashima, M. Iwane, O. Matsuda, and K. Murase, J. Cryst. Growth **127**, 1041 (1993).

[5] M. Ogawa, M. Itoh, and T. Miyoshi, Physica B **227**, 65 (1996).
[6] Z.-L. Ji and K.-F. Berggren, Phys. Rev. B **45**, 6652 (1992).
[7] C. S. Lent and D. J. Kirkner, J. Appl. Phys. **67**, 6353 (1990).
[8] M. Leng and C. S. Lent, J. Appl. Phys. **76**, 2240 (1994).
[9] J. M. Luttinger and W. Kohn, Phys. Rev. **97**, 869 (1955).
[10] U. Bockelmann and G. Bastard, Phys. Rev. B **45**, 1688 (1992).
[11] C. Y. P. Chao and S. L. Chuang, Phys. Rev. B **43**, 7027 (1991). Note that the authors' formulation is same as theirs, but their result [Eq. (18a)–(18c)] in the literature is somewhat erroneous.
[12] C. Lanczos, J. Res. Natl. Bur. Stand. **45**, 255 (1950).
[13] H. Ando, S. Nojima, and H. Kanbe, J. Appl. Phys. **74**, 6383 (1993).